MECHANISM OF LONG-PERIOD STRUCTURAL MODULATIONS IN $A'A''BX_4$ COMPOUNDS*

M. KURZYŃSKI

Institute of Physics, A. Mickiewicz University
Matejki 48, PL-60-769 Poznań, Poland

(Received January 9, 1995)

A simple lattice model with two Ising spins is proved to explain practically all structural phase transitions observed in almost 40 different $A'A''BX_4$ compounds. Ising variables describe four discrete orientational states of BX_4 tetrahedra. Symmetrical nearest-neighbour interactions between spins stabilize crystallographic structures with up to four formula units per elementary cell. Longer-period, as well as incommensurate modulations of the order parameter, both along the hexagonal axis and in the perpendicular plane, originate either from symmetrical next-nearest-neighbour or, competitively, antisymmetrical nearest-neighbour interactions.

PACS numbers: 05.50. +q, 64.60. Cm, 64.70. Rh

1. Introduction

In this review we discuss long-period, also incommensurate, structural modulations observed in a large number of compounds of a general chemical formula $A'A''BX_4$ [1–3]. The compounds under consideration form ionic crystals with A' and A'' being singly charged cations and BX_4, doubly charged anions. Apart from compounds composed of cations that are extremely small when compared to anions (Li_2SO_4, $LiNaSO_4$, Na_2SO_4 and some iodide salts), crystallographic structures of all other known $A'A''BX_4$ compounds can be considered as slight distortions of the prototype α-K_2SO_4 structure of $P6_3/mmc$ symmetry (Fig. 1). In the prototype structure the

* Presented at the VII Symposium on Statistical Physics, Zakopane, Poland, September 22–28, 1994.

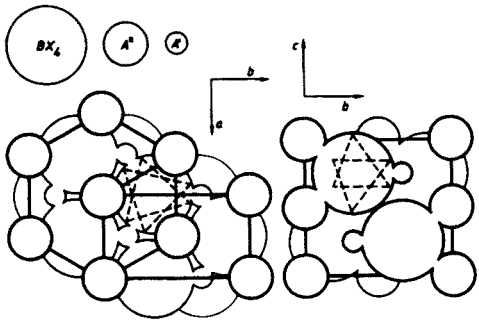

Fig. 1. Nonpolar and nondistorted α-K_2SO_4 structure of $P6_3/mmc$ symmetry as projected along the c and a axes. The same notation of the axes is used throughout the paper. Hexagonal ($Z = 2$) and orthorhombic ($Z = 4$) unit cells are shown. Relative magnitudes of ions apply approximately to $A' = Li^+$, $A'' = K^+$, and $BX_4 = SO_4^{2-}$. Note the impossibility of free rotation of BX_4 tetrahedra. The projection of four different sterically allowed orientations of the tetrahedra is shown. They are labelled with the help of two Ising variables: $\sigma = \pm 1$ (position with the apex up or down, respectively) and $\tau = \pm 1$ (turn to the right or left, respectively). After Ref. [4].

BX_4 tetrahedra are oriented at random. A variety of experimentally observed structural phase transitions result from various orientational orderings of BX_4 groups accompanied by ionic displacements.

In the prototype crystallographic structure the anions BX_4 form a hexagonal close-packed (hcp) structure of spheres (Fig. 2). The cations A'' occupy octahedral interstitial sites in between the spheres, whereas the cations A' occupy pairs of tetrahedral interstitial sites combined into single cages. The cations A' larger than lithium fit these cages only after an expansion of the whole structure in a plane perpendicular to to the hexagonal axis. In consequence, for most $A'A''BX_4$ compounds the c/a ratio of the prototype unit cell (compare Fig. 1) is considerably smaller than the value $\sqrt{8/3} \approx 1.63$ for the ideal hcp structure.

Each BX_4 anion is surrounded by five A' and six A'' cations. There are twelve different equivalent orientations with the minimum potential energy of BX_4 tetrahedron in such a cationic environment. They can be grouped into four discrete orientational states labeled with the help of two Ising variables σ and τ. The variable $\sigma = \pm 1$ describes the positions of the tetrrahedron with the apex up or down, respectively, the c axis, whereas the variable $\tau = \pm 1$ describes the turns of the tetrahedron about the c axis to the right or to the left (Fig. 1). In a rigid lattice transitions between the states (σ, τ) are sterically forbidden and become possible only after taking into account the lattice vibrations.

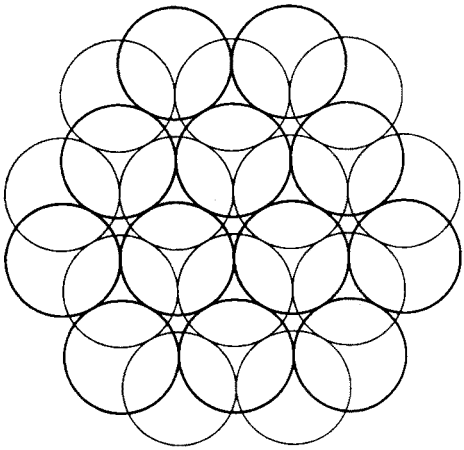

Fig. 2. Hexagonal close-packed structure of spheres projected onto the hexagonal plane. Octahedral and tetrahedral interstitial sites are seen.

Three orientations of minimum energy within each of the four states (σ, τ) correspond to slight tiltings of the trigonal axis of the tetrahedron in three distinct vertical planes rotated mutually by 120° around the c axis. The energy barrier that has to be overcome while changing the direction of tilting is not of steric nature and rather low. Since in all but one (phase transition in $LiKSO_4$ at 190 K) cases studied so far the order in (σ, τ) states automatically distingushes particular tiltings there is no need to consider the additional substates explicitely.

The statistical model with orientational states of BX_4 tetrahedra described with the help of two Ising spins was proposed by the author and his coworker, Mohamed Halawa, in 1986 [4]. The model appeared to be able to explain practically all the structural phase transitions observed in $A'A''BX_4$ compounds with the prototype α-K_2SO_4 structure [3]. The aim of the present paper is to present in some detail the particular interactions between spins which are responsible for longer-period or incommensurate structural modulations, both along the hexagonal axis and in the hexagonal plane.

2. Experimental data

Nowadays, almost 40 different $A'A''BX_4$ compounds occurring in the prototype α-K_2SO_4 ($P6_3/mmc$) or β-K_2SO_4 ($Pmcn$) high-temperature phases are known to undergo various structural phase transitions with falling temperature. The essential reliable experimental information is collected in Figs 3 to 5. Seven classes, I to VII, of the compounds are distinguished.

I

	$Pmcn\ (Z=4)$ ferroelastic	$P6_3/mmc\ (Z=2)$
K_2SO_4	860	
Rb_2SeO_4	822	

	$Pmcn\ (Z=4)$ ferroelastic	q along b^* incommens.	$P6_3/mmc\ (Z=2)$
K_2MoO_4	593		733
K_2WO_4	643		707
Rb_2WO_4	681		753

II

	$C1c1\ (Z=24)$ ferroelectr. c	$P2_1cn\ (Z=12)$ ferroelectr. a	$q=(1-\delta)c^*/3$ incommens.	$Pmcn\ (Z=4)$ ferroelastic	$P6_3/mmc\ (Z=2)$
K_2SeO_4		93	130	745	
Rb_2CoCl_4	66	192	295		
Rb_2ZnCl_4	74	192	303		
Rb_2CoBr_4		193	333		
Rb_2ZnBr_4		* 194	347		
K_2ZnCl_4	145	403	553		
K_2CoCl_4	142				
K_2ZnBr_4		290	561		
K_2CoBr_4		300	555		

	$P2_1cn\ (Z=12)$ ferroelectr. a	$Pc2_1n\ (Z=16)$	$q=(1+\delta)c^*/4$ incommens.	$Pmcn\ (Z=4)$
$(NH_4)_2ZnCl_4$	268	* 364		406
$(NH_4)_2ZnBr_4$	217	395		432

Fig. 3. Phases observed in Classes I and II of $A'A''BX_4$ compounds. Transition temperatures are in kelvins. Two phase transitions without a change in the modulation vector are marked by an asterisk. These are a first order transition from $P2_1cn$ ($Z=12$) to $P1c1$ ($Z=12$) phase in Rb_2ZnBr_4 below 76 K, and a first order transition from $Pc2_1n$ ($Z=16$) to $Pc11$ ($Z=16$) or $P21/c1$ ($Z=16$) phase in $(NH_4)_2ZnCl_4$ below 319 K.

Transition temperatures are given in kelvins. Apart from the space symmetry group and a number Z of formula units per elementary cell or (in the case of incommensurate structures) a value of the modulation vector q, also ferroic properties, if present, of each phase are included. References to a huge experimental literature comprising more than thousand items can be found in the reviews by Cummins [1] (only compounds with incommensurate phases), Tomaszewski [2] and Kurzyński [3].

III

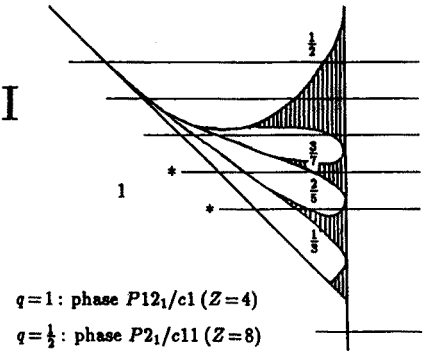

T_2NiCl_4 (221 – 275 – 283)
T_2MnCl_4 (172 – 267 – 291 – 292)
T_2FeCl_4 (240 – 266 – 267 – 270 – 281)
T_2ZnCl_4 (168 – 275 – 280 – 296)
T_2CoCl_4 (192 – 276 – 280 – 281 – 293)

$q=1$: phase $P12_1/c1$ ($Z=4$)
$q=\frac{1}{2}$: phase $P2_1/c11$ ($Z=8$)
$q=\frac{2}{7}$: phase $P2_12_12_1$ ($Z=28$)
$q=\frac{2}{5}$: phase $P2_1cn$ ($Z=20$)
$q=\frac{1}{3}$: phase $P112_1/n$ ($Z=12$)

T_2CdBr_4 (272), T_2HgCl_4 (278),
T_2CoBr_4 (287), T_2ZnBr_4 (288)

IV

	$Pbc2_1$ ($Z=8$)	$P12_1/c1$ ($Z=4$)	$Pmcn$($Z=4$)
	ferroroelectr. c	ferroelastic	
T_2ZnI_4	210	254	

	$P12_1/c1$ ($Z=4$)	$Pbc2_1$ ($Z=8$)	$q=(1+\delta)\,b^*/2$	$Pmcn$($Z=4$)
	ferroelastic	ferroroelectr. c	incommens.	
T_2CuBr_4	237	242	272	

	$Pbc2_1$ ($Z=8$)	$Pmcn$($Z=4$)
	ferroroelectr. c	
T_2CdI_4	240	

Fig. 4. Phases observed in Classes III and IV, composed of T_2BX_4 compounds with T denoting tetramethylammonium, $N(CH_3)_4$. Transition temperatures are in kelvins. Data for Class III are presented in the form of experimental "phase diagram". For this case, successive transition temperatures are given in brackets, and the modulation vectors for commensurate phases in units of the reciprocal lattice constant c^*. The shaded area corresponds to incommensurate modulations. The vertical line represents transition to $Pmcn$ ($Z=4$) phase. Proportions between particular temperature ranges are not kept. Not shown, but marked by an asterisk are transitions to the alternative phase with $q=1/3$, $P2_12_12_1$ ($Z=12$), observed in T_2ZnCl_4 and T_2CoCl_4 below 155 K and 122 K, respectively. In four compounds T_2CdBr_4, T_2HgCl_4, T_2CoBr_4, and T_2ZnBr_4 a direct transition from $Pmcn$ ($Z=4$) to $P12_1/c1$ ($Z=4$) phase occurs.

V

	$P112_1/n\,(Z=4)$ ferroelastic	$P12_1/c1\,(Z=12)$ ferroelastic	$q=(1-\delta)c^*/3$ incommens.	$Pmcn\,(Z=4)$
T_2CuCl_4	263	292		298

	$P\bar{1}\,(Z=4)$ ferroelastic	$P112_1/n\,(Z=4)$ ferroelastic	$q=\delta c^*$ incommens.	$Pmcn\,(Z=4)$
Cs_2HgBr_4	165	230	243	
Cs_2CdBr_4	158	237	252	
Cs_2CdI_4	183	260	332	

	$P112_1/n\,(Z=4)$ ferroelastic	$Pmcn\,(Z=4)$
$LiCsSO_4$	201	

	$P112_1/n\,(Z=4)$ ferroelastic	$P11n\,(Z=20)$ ferroelectr. a	$P2_1/c11\,(Z=8)$ ferroelastic	$P2_1cn\,(Z=28)$ ferroelectr. a	$q=2(1-\delta)c^*/5$ incommens.	$Pmcn\,(Z=4)$
$LiRbSO_4$	438	457	472.7	473.1	474.5	

	$C1c1\,(Z=16)$	$P2_1/c11\,(Z=8)$ ferroelastic	$P2_1cn\,(Z=4)$ ferroelectr. a	$Pmcn\,(Z=4)$
$LiNH_4SO_4$	27	283	460	

VI

	?	$Cc\,(Z=4)$ ferroelastic	$P31c\,(Z=2)$ pyroelectr. c	$P6_3\,(Z=2)$ pyroelectr. c	q in a^*b^* plane ferroelastic	$P6_3/mmc\,(Z=2)$
$LiKSO_4$	135	190	hysteresis 205–250	708	943	
$LiRbCrO_4$			550	606	843	

VII

	$P\bar{3}m1\,(Z=2)$	
$NaKSO_4$	453?	

Fig. 5. Phases observed in Classes V, VI and VII of $A'A''BX_4$ compounds. Transition temperatures are in kelvins. $T \equiv N(CH_3)_4$.

3. Four-sublattice ordering

In the four-dimensional space spanned by the states (σ, τ) of a single tetrahedron there are four operators I (unit), σ, τ and $\sigma\tau$ that are *diagonal*, *i.e.* do not change these states. We are not going to deal with dynamics of orientational states, so we confine our attention only to these diagonal operators. The space of orientational states of a pair of BX_4 tetrahedra is $4 \times 4 = 16$-dimensional and the spectrum of values of the interaction energy in these states is in general determined by a combination of 16 possible products of operators I, σ, τ and $\sigma\tau$ attached to the corresponding tetrahedra. Such a combination must be invariant with respect to the local symmetry group of the pair.

There are two inequivalent nearest-neighbour (nn) pairs of sites in the hcp structure: those that lie in and those that lie out of the plane perpendicular to the hexagonal axis (Fig. 6). Symmetry conditions reduce the most general Hamiltonian of nearest-neigbour orientational interactions to the form [4]

$$\begin{aligned}\mathcal{H}^{\mathrm{nn}} = & J \sum_{\mathrm{nn\ in}} \sigma_i\sigma_j + K \sum_{\mathrm{nn\ in}} \tau_i\tau_j + L \sum_{\mathrm{nn\ in}} \sigma_i\tau_i\sigma_j\tau_j \\ & + J' \sum_{\mathrm{nn\ out}} \sigma_i\sigma_j + K' \sum_{\mathrm{nn\ out}} \tau_i\tau_j + L' \sum_{\mathrm{nn\ out}} \sigma_i\tau_i\sigma_j\tau_j \\ & + \tfrac{1}{2}M \sum_{\mathrm{nn\ in}} \sigma_i\sigma_j(\tau_i - \tau_j) + \tfrac{1}{2}M' \sum_{\mathrm{nn\ out}} \tau_i\tau_j(\sigma_i - \sigma_j)\,. \qquad (1)\end{aligned}$$

In Eq. (1), "nn in" and "nn out" denote summation over nearest neighbours lying in and out of the hexagonal planes, respectively. Each pair in the sum is assumed to be counted singly.

The interaction between spins can be either direct (purely electrostatic, mainly octupole-octupole interaction between BX_4 tetrahedra) or indirect (coupling of orientations through ionic translations, both static and dynamic). The latter interaction is responsible for particular orientational orderings being accompanied by specific lattice distortions. Because of the number of parameters (note that the Hamiltonian (1) includes only the nearest-neighbour interaction) any attempt at quantitative fit of the theory to experimental data is in general methodologically meaningless. Consequently, it is sufficient to study thermodynamics of the model only qualitatively, in the simplest molecular-field approximation (MFA).

The nn interaction on the hcp structure in, *e.g.*, the σ Ising subsystem:

$$\mathcal{H}^{\mathrm{nn}\sigma} = J \sum_{\mathrm{nn\ in}} \sigma_i\sigma_j + J' \sum_{\mathrm{nn\ out}} \sigma_i\sigma_j \qquad (2)$$

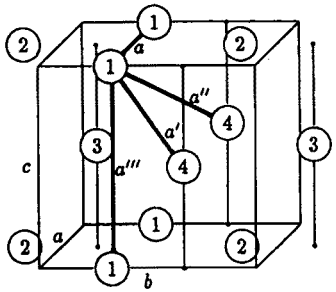

para, P:
$m_1 = m_2 = m_3 = m_4 = 0$
ferro, F:
$m_1 = m_2 = m_3 = m_4 \neq 0$
antiferro A:
$m_1 = m_2 = -m_3 = -m_4$
antiferro B:
$m_1 = -m_2 = -m_3 = m_4$
antiferro C:
$m_1 = -m_2 = m_3 = -m_4$

Fig. 6. Geometry of the hcp structure. Orthorhombic ($Z = 4$) unit cell is shown. There are two kinds of nearest neighbours distanced by a and a', respectively ($a = a'$ for the ideal hcp structure with $c = \sqrt{8/3} \approx 1.63a$), and two kinds of next-nearest neighbours distanced by a'' and $a''' \equiv c$, respectively ($a'' = a'''$ for the hcp structure shrunk along the hexagonal axis in such a way that $c/a = 4/3 \approx 1.33$, which is approximately the case for most $A'A''BX_4$ compounds). Labelling of four sublattices is indicated and five possible orderings are listed.

can stabilize at most a four-sublattice structure of ordering (Fig. 6). The molecular-field theory with the four order parameters

$$m_s \equiv \langle \sigma_i \rangle_{i \in s}; \quad s = 1,\ 2,\ 3,\ 4\,, \tag{3}$$

(the brackets $\langle \ldots \rangle$ mean the self-consistent canonical ensemble average) provides five possible orderings: a para (P) phase, $m_s = 0$, a ferro (F) ordering, $m_s = 1$, and three types of antiferro orderings A, B, and C (Fig. 6). The molecular-field theory for the entire Hamiltonian (1) with the four additional order parameters

$$n_s \equiv \langle \tau_i \rangle_{i \in s}; \quad s = 1,\ 2,\ 3,\ 4\,, \tag{4}$$

considered by the author and Mohamed Halawa [4] determined regions of stability of 25 generally possible phases: PP, PF, ... BC, BC, where the first and the second letter correspond to the order of the variable $\langle \sigma \rangle$ and $\langle \tau \rangle$, respectively.

Assuming at most four-sublattice ordering and the approximation

$$\langle \sigma_i \tau_i \rangle = \langle \sigma_i \rangle \langle \tau_i \rangle\,, \tag{5}$$

antisymmetrical coupling terms with the parameters M and M' in the Hamiltonian (1) do not contribute to the mean-field energy. However, the effect of symmetrical coupling terms with the parameters L and L' does not vanish. In the approximation (5), it consists formally in a replacement of the parameters J, J' and K, K' of the interaction within, respectively, the σ and the τ subsystem, by the effective temperature-dependent parameters [5]:

$$J_{\text{eff}} = J + \langle \tau_i \tau_j \rangle L, \quad J'_{\text{eff}} = J' + \langle \tau_i \tau_j \rangle L'\,, \tag{6}$$

and

$$K_{\text{eff}} = K + \langle \sigma_i \sigma_j \rangle L, \quad K'_{\text{eff}} = K' + \langle \sigma_i \sigma_j \rangle L' . \tag{7}$$

Only 8 of 25 possible orderings have been observed so far in $A'A''BX_4$ compounds. They are given and identified in Table I. In Table II, all experimentally observed transitions between phases determined by the four-sublattice model are listed. The symmetrical σ-τ coupling allows various sequences of successive phase transitions with temperature, and makes some transitions discontinuous. This is also the origin of a change of sign with temperature of the effective K' interaction, Eq. (7), which explains a change of the τ-ordering from ferro to antiferro one observed in the Class VI compounds $LiKSO_4$ and $LiRbCrO_4$ (Table II). A discontinuity of τ-para to τ-ordered phase transition originated from the symmetrical σ-τ coupling can explain the lack of τ-ordering, observed down to the very low temperatures in the Class I compounds, Fig. 3, as a consequence of a possible large hysteresis.

TABLE I

Experimentally observed crystallographic phases with up to four formula units per elementary cell.

hexagonal $P6_3/mmc\,(Z=2)$	PP	prototype observed only in Classes I, II, VI
hexagonal $P6_3\,(Z=2)$	FF	Class VI
trigonal $R31c\,(Z=2)$	FA	Class VI
trigonal $R\bar{3}m1\,(Z=2)$	AP	Class VII ($NaKSO_4$)
orthorhombic $Pmcn\,(Z=4)$	BP	all compounds except Classes VI and VII
orthorhombic $P2_1cn\,(Z=4)$	BA	$LiNH_4SO_4$ and Rb_2BeF_4
monoclinic $P112_1/n\,(Z=4)$	BF	Class V except $LiNH_4SO_4$ and Rb_2BeF_4
monoclinic $P12_1/c1\,(Z=4)$	BC	Classes III and IV (T_2BX_4 compounds)

TABLE II

Experimentally observed transitions (with falling temperature) between phases determined by the four-sublattice model.

PP $\rightarrow$ BP	Classes I and II
BP $\rightarrow$ BC	Classes III and IV
BP $\rightarrow$ BF or BA	Class V
PP $\rightarrow$ FF $\rightarrow$ FA	Class VI
? $\rightarrow$ AP	Class VII

4. Longer-period modulations along the hexagonal axis. The ANNNI model and its derivatives

Longer-period, also incommensurate modulations of the structure along the hexagonal c axis have been observed in the Classes II, III and V of $A'A''BX_4$ compounds (Figs 3 to 5). Two mechanisms responsible for stabilizing such modulations are possible. The first, proposed by Yamada and Hamaya in 1983 [6], is a competition of interactions between nearest and further distanced τ (in our notation) spins.

On distinguishing explicitely the nearest- and the next-nearest-neighbour τ-τ interactions along the c axis at distances denoted in Fig. 6 as a' and a''', respectively, one obtains an orientational Hamiltonian

$$\mathcal{H}^{\mathrm{ANNNI}} = K' \sum_{\mathrm{nn}'} \tau_i \tau_j + K''' \sum_{\mathrm{nnn}'''} \tau_i \tau_j + \text{remaining interactions}, \tag{8}$$

of the form of the well-known ANNNI (axial next-nearest-neighbour Ising) model [7, 8]. Assuming that interactions not explicitely mentioned in Eq. (8) secure ferro or antiferro τ-ordering in hexagonal planes, and that each plane can form a separate sublattice, labelled with an index l, the MFA free energy for the Hamiltonian (8) is of the form

$$\begin{aligned} F^{\mathrm{ANNNI}}/N = &\sum_l \left(K_0 n_l^2 + K_1 n_l n_{l+1} + K_2 n_l n_{l+2}\right) \\ &+ \tfrac{1}{2} kT \sum_l [(1+n_l)\ln(1+n_l) + (1-n_l)\ln(1-n_l) - 2\ln 2]. \end{aligned} \tag{9}$$

In Eqs (9), N is the number of sites in each plane. The parameters K_1 and K_2 depend not only on the parameters K' and K''', but also (self-consistently) on parameters of the remaining interactions and on temperature. We are not, however, going to deal with a particular form of this dependence here. An additional K_0 term controls the degree of τ-spin ordering in hexagonal planes. Its value is determined mainly by the value of parameter K characterizing the in-plane nn interaction between τ spins.

Minimization of the free energy (9) leads to a set of self-consistent equations

$$\begin{aligned} &2K_0 n_l + K_1(n_{l-1} + n_{l+1}) + K_2(n_{l-2} + n_{l+2}) \\ &\quad + \tfrac{1}{2} kT\,[\ln(1+n_l) - \ln(1-n_l)] = 0. \end{aligned} \tag{10}$$

It is easy to show that Eqs (10) have solutions describing long-range modulations of the order parameter n_l. Indeed, for small values of n_l's (*i.e.*, in the

vicinity of a continuous phase transition) these equations can be linearized, $\ln(1 \pm n_l) \approx \pm n_l$, and, after introducing the Fourier transforms:

$$n_q \equiv \sum_l \mathrm{e}^{-iql} n_l \,, \tag{11}$$

one gets, for $n_q \neq 0$, the equation:

$$kT = -2K_0 - 2K_1 \cos q - 2K_2 \cos 2q \,. \tag{12}$$

This determines the temperature of a continuous phase transition of the order-disorder type. For positive (antiferro) K_2, within the range of parameters $-4K_2 \leq K_1 \leq 4K_2$, a value of the modulation vector q that maximizes the temperature (12) varies continuously from 0 to π according to the equation

$$\cos q = -K_1/4K_2 \,, \tag{13}$$

and only outside this region is q constant, taking the value either 0 or π. The latter means that points $K_1 = \pm 4K_2$, corresponding to the transition temperature $kT = 6K_2 - 2K_0$, are Lifshitz points [7].

Eq. (10) can be considered as a recurrence relation describing a discrete 4-dimensional mapping:

$$(n_{l-2}, n_{l-1}, n_l, n_{l+1}) \rightarrow (n_{l-1}, n_l, n_{l+1}, n_{l+2}) \,. \tag{14}$$

Numerical solutions with boundary conditions $n_{l+L} = n_l$ for finite, not very large values of L, and the soliton approximation in regions close to the order-disorder continuous transition lead, comparing corresponding values of the free energy, to the phase diagram given in Fig. 7 [7, 8]. In Fig. 8 it is shown that the model describes qualitatively all, except for the few marked in Figs 3 and 4 with an asterisk, sequences of transitions between phases modulated along the c axis observed in compounds of the Classes II, III and V. Slopes of the lines determining successive transitions can be explained as being due to a temperature dependence of the effective parameters K_1 and K_2. We are not going to study any particular form of this dependence but let us point out that it originates mainly from a coupling to the σ spin subsystem (determined by the parameter L', see Eq. (7)).

Stabilization of the phase $q = \frac{2}{3}$ (in units c^*) at $T = 0$ observed in the Class II compounds and destabilization of that phase observed in $LiRbSO_4$ can be considered as resulting from the third-neighbour interaction or a coupling to a static strain [6]. There are, however, also other ways to change the phase diagram in Fig. 7.

The free energy (9) can be rewritten in terms of a generalized "action integral" [9]:

$$F^{\mathrm{ANNNI}}/N = \sum_l \left[-\tfrac{1}{2} K_1 (n_{l+1} - n_l)^2 - \tfrac{1}{2} K_2 (n_{l+2} - n_l)^2 + V(n_l) \right] \tag{15}$$

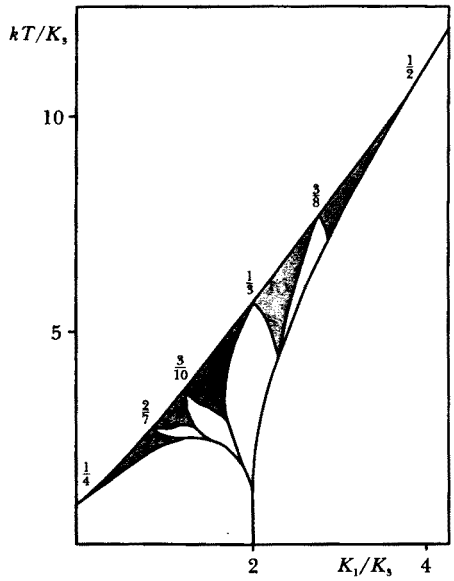

Fig. 7. Phase diagram of the ANNNI model in the MFA, Eq. 9, for $K_0 = -2|K_1|$. Values of the modulation vector of main commensurate phases are given in units of the reciprocal lattice vector 2π. The shaded area corresponds to longer-period commensurate as well as incommensurate phases. Only the half-plane $K_1 > 0$ is shown. The half-plane $K_1 < 0$ is a mirror image of the former with respect to the axis $K_1 = 0$; in this range the modulation vectors q should be replaced by $\frac{1}{2} - q$. The vector $q = \frac{1}{2}$ describes the antiferro ordering whereas the vector $q = 0$, the ferro one. After Ref. [7], redrawn in dimensionless coordinates referred to the nnn interaction parameter $K_2 > 0$.

with the index l having the meaning of discrete time and, for $K_0 = 0$, the "potential energy"

$$V(n) = (K_1 + K_2)\, n^2 + \tfrac{1}{2} kT\, [(1+n)\ln(1+n) + (1-n)\ln(1-n)]\,. \quad (16)$$

Taylor expansion of Eq. (16) up to the forth power:

$$V(n) = \left(K_1 + K_2 + \frac{kT}{2}\right) n^2 + \frac{kT}{12} n^4 + \cdots, \quad (17)$$

reconstructs the model considered by Janssen and Tjon [10] and called by them the DIFFOUR (discrete frustrated φ^4) model. In the original notation of these authors:

$$x_l \equiv \sqrt[4]{kT/3}\, n_l, \quad A \equiv \sqrt{3kT}, \quad B \equiv K_1 \sqrt{3/kT}, \quad D \equiv K_2 \sqrt{3/kT}\,, \quad (18)$$

the free energy (15), (17) reads

$$F^{\mathrm{DIFFOUR}}/N = \sum_l \left[\tfrac{A}{2} x_l^2 + \tfrac{1}{4} x_l^4 + B x_l x_{l+1} + D x_l x_{l+2}\right]. \quad (19)$$

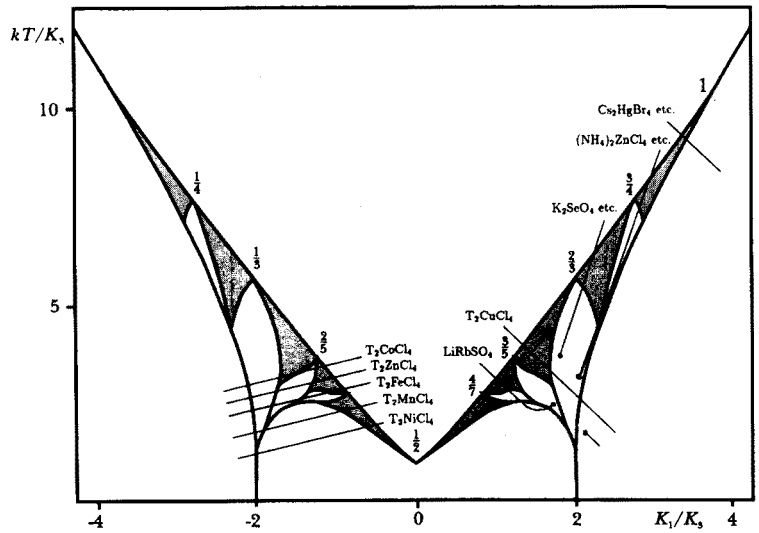

Fig. 8. The ANNNI model. Qualitative fitting of sequences of transitions between phases modulated along the c axis observed in the Class II, III and V compounds. Slopes of the lines connecting the successive transitions are due to temperature dependence of the effective parameters K_1 and K_2. This dependence originates mainly from a symmetrical coupling to the σ spin subsystem. Values of the modulation vector are referred to the reciprocal lattice vector c^* of the prototype hcp structure (Figs 1 or 6; since there are two haxagonal layers of BX_4 tetrahedra per the unit cell constant c, the dimensionless reciprocal lattice vector 2π corresponds to $2c^*$). We assume that the modulation vector q belongs to the extended Brillouin zone rather than to the reduced one as in Figs 3 to 5. For acoustic modes of modulation (Class III compounds) both vectors coincide, $q_{\text{ext}} = q_{\text{red}}$, whereas for optical modes of modulation (Class II and V compounds), they are related by equation $q_{\text{ext}} = c^* - q_{\text{red}}$. The phase with $q = \frac{2}{3}c^*$ is stable down to the very low temperatures in the Class II compounds whereas in $LiRbSO_4$ it does not occur at all.

The corresponding phase diagram in the coordinates $B/D \equiv K_1/K_2$ and $A/D \equiv kT/K_2$ [11] is given in Fig. 9. Jannsen [12] showed that the semimicroscopic DIFFOUR model describes modulated phases in $A'A''BX_4$ compounds as well as the generalized ANNNI model proposed by Yamada and Hamaya [6].

Still another model that could be interpreted as a derivative of the ANNNI model was considered by Villain and Gordon [13], and Axel and Aubry [14]. In appriopriately normalized variables $u_l \propto n_l$ one can rewrite and approximate the double-well potential (17) according to the formula

$$V(u) = \tfrac{1}{8}(u^2-1)^2 - \tfrac{1}{2}c_0u^2 \approx \tfrac{1}{2}(u-\sigma)^2 - \tfrac{1}{2}c_0u^2\,, \qquad (20)$$

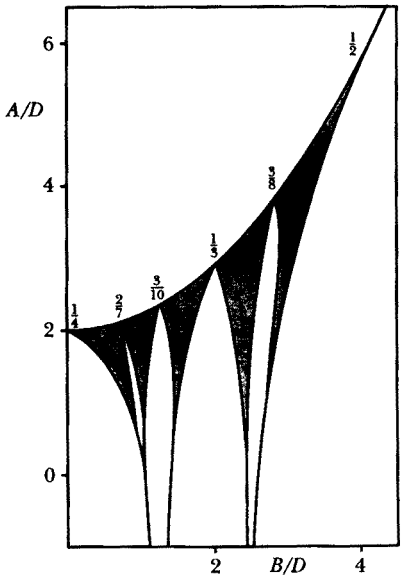

Fig. 9. Phase diagram of the DIFFOUR model, Eq. (19). The modulation vectors of main commensurate phases are given in units of 2π. The shaded area corresponds to longer-period commensurate as well as incommensurate phases. Dimensionless coordinates B/D and A/D correspond, respectively, to dimensionless coordinates K_1/K_2 and kT/K_2 in Fig. 7. The half-plane $B/D < 0$ is a mirror image of the half-plane $B/D > 0$. Redrawn after Ref. [11].

where c_0 is a parameter and σ denotes the sign of u,

$$\sigma \equiv \text{sign}(u) = \pm 1 . \tag{21}$$

The total free energy (15) than takes the form

$$F^{\text{ELRII}}/N = \tfrac{1}{2} \sum_l \left[-c_0 u_l^2 + c_1 (u_{l+1} - u_l)^2 + c_2 (u_{l+2} - u_l)^2 + (u_l - \sigma_l)^2 \right] , \tag{22}$$

where c_0, c_1 and c_2 are three independent parameters. The trick of Villain and Gordon [13] and Axel and Aubry [14] was to consider σ as a variable completely independent of u. On minimizing Eq. (22) with respect to u_l and performing the Fourier transformation as in Eq. (11), one gets a linear relation $u_q \propto \sigma_q$ which, when put back after the inverse Fourier transformation into Eq. (22), results in an expression having the meaning of a Hamiltonian of some long-range interaction between Ising spins σ_l. The so obtained ELRII (effective long-range interaction Ising) model was studied numerically for finite temperatures in the MFA by Mashiyama [15] and, later on, applied for description of modulated phases of $A'A''BX_4$ compounds by Kawamura

et al. [16]. Fig. 10 presents the phase diagram of the ELRII model for $c_0 = \frac{1}{2}$. It is seen that also this model describes qualitatively all sequences of transitions between modulated phases observed in the Classes II, III and V of $A'A''BX_4$ compounds, except those few marked in Figs 3 and 4 with an asterisk.

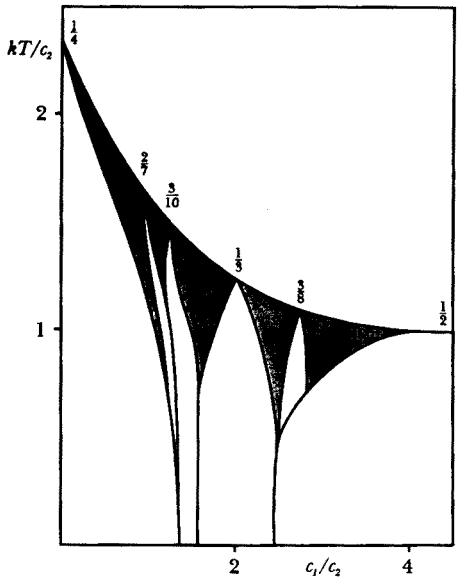

Fig. 10. Phase diagram of the ELRII model, Eq. (22), for $c_0 = \frac{1}{2}$. The modulation vectors of main commensurate phases are given in units of 2π. The shaded area corresponds to longer-period commensurate as well as incommensurate phases. The half-plane $c_1 < 0$ is a mirror image of the half-plane $c_1 > 0$. After Ref. [15], redrawn after Ref. [16].

5. Longer-period modulations along the hexagonal axis. The AANNDI model

The second, alternative mechanism of stabilizing longer-period modulations of structure along the hexagonal axis in $A'A''BX_4$ compounds was proposed by the author of the present review and his coworkers [5, 17, 18]. The essential role in this mechanism is played by the nearest-neighbour out-of-plane antisymmetrical M' interaction in the Hamiltonian (1). Formally, the existence of this as well as the in-plane antisymmetrical M interaction result from the lack of the centre of symmetry for nn pairs on the hcp structure. The strengths of both interactions can be evaluated by comparing

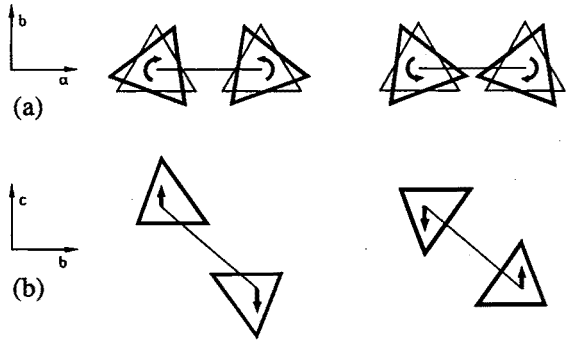

Fig. 11. Two configurations of nn pairs of BX_4 tetrahedra in (a) and out (b) of hexagonal plane (b). Their energies differ by the term of antisymmetrical interaction $\frac{1}{2}M\sigma_1\sigma_2(\tau_1 - \tau_2)$ (a) and $\frac{1}{2}M'\tau_1\tau_2(\sigma_1 - \sigma_2)$ (b). After Ref. [18].

electrostatic energies of different configurations of nn pairs of BX_4 tetrahedra drawn schematically in Figs 11 (a) and (b).

Both antisymmetrical terms in the Hamiltonian (1) contribute to the MFA free energy only when the assumed ordering is more complex than the four-sublattice one (compare Section 3). Like the models of longer-period modulations considered in Section 4, also the models with antisymmetrical interactions can be named with the help of several-letter abbreviations. Thus, we have proposed [18] to call a statistical model involving the out-of-plane M' term, the AANNDI (axial antisymmetrical nearest-neignbour double Ising) model, and that involving the in-plane M term, the PANNDI (planar antisymmetrical nearest-neighbour double Ising) model.

The simplest non-trivial version of AANNDI model distinguishes explicitely two terms and is described by the Hamiltonian

$$\mathcal{H}^{\mathrm{AANNDI}} = K' \sum_{\mathrm{nn}'} \tau_i\tau_j + \tfrac{1}{2}M' \sum_{\mathrm{nn}'} \tau_i\tau_j(\sigma_i - \sigma_j) + \text{remaining interactions}, \tag{23}$$

where "nn′ " denotes the same as "nn out" in Eq. (1), *i.e.* summation over the nearest neighbours lying out of the hexagonal plane (distanced by a' in Fig. 6). Also in this case we assume at first that interactions not explicitely mentioned in Eq. (23) secure appropriate ferro or antiferro orderings in hexagonal planes. Under such an assumption and denoting

$$\omega_i \equiv \sigma_i\tau_i, \qquad r_s \equiv \langle\omega_i\rangle_{i\in s}, \tag{24}$$

we find the most general MFA free energy for the Hamiltonian (23) to be

$$F^{\mathrm{AANNDI}}/N = K_1 \sum_l n_l n_{l+1} + \tfrac{1}{2} M_1 \sum_l (r_l n_{l+1} - n_l r_{l+1})$$
$$+ \tfrac{1}{2} kT \sum_l [(1+n_l)\ln(1+n_l) + (1-n_l)\ln(1-n_l) - 2\ln 2]$$
$$+ \tfrac{1}{2} kT \sum_l [(1+r_l)\ln(1+r_l) + (1-r_l)\ln(1-r_l) - 2\ln 2] , \tag{25}$$

where N is the number of sites in each plane. The free energy (25) does not vanish only if τ- and ω-orderings in the hexagonal planes are both of ferro or antiferro type. The parameters K_1 and M_1 depend on the parameters K' and M' and (selfconsistently) on parameters of the remaining interactions as well as temperature. We shall not study any specific form of this dependence here.

Minimization of the free energy (25) with respect to n_l's and r_l's leads to a set of self-consistent equations

$$K_1(n_{l-1} + n_{l+1}) + \tfrac{1}{2} M_1 (r_{l-1} - r_{l+1}) + \tfrac{1}{2} kT [\ln(1+n_l) - \ln(1-n_l)] = 0 ,$$
$$- \tfrac{1}{2} M_1 (r_{l-1} - r_{l+1}) + \tfrac{1}{2} kT [\ln(1+r_l) - \ln(1-r_l)] = 0 . \tag{26}$$

Eqs (26), like Eqs (10), have solutions describing long-range modulations of the order parameter n_l (as well as r_l). Indeed, after linearization and introducing the Fourier transforms n_q and r_q one gets, from the condition of a non-zero solution, an equation for the continuous phase transition temperature:

$$kT = -K_1 \cos q + \sqrt{K_1^2 \cos^2 q + M_1^2 \sin^2 q} . \tag{27}$$

The sign of M_1 has no physical meaning; we assume it as positive. To maximize expression (27), the modulation vector has to be $q = 0$ for $K_1 < -M_1/\sqrt{2}$ and $q = \pi$ for $K_1 > M_1/\sqrt{2}$. Within the range $-M_1/\sqrt{2} \leq K_1 \leq M_1/\sqrt{2}$ the maximizing value of q varies continuously from 0 to π according to the equation

$$\cos q = -K_1/\sqrt{M_1^2 - K_1^2} . \tag{28}$$

Points $K_1 = \pm M_1/\sqrt{2}$, corresponding to the temperature $kT = \sqrt{2} M_1$, are Lifshitz points.

In general, Eqs (26) can be considered as a recurrence relation describing a discrete 4-dimensional nonlinear mapping:

$$(n_{l-1}, r_{l-1}, n_l, r_l) \to (n_1, r_l, n_{l+1}, r_{l+1}) . \tag{29}$$

They have been solved numerically by Bartkowiak [18] for periodic boundary conditions $n_{l+L} = n_l$, $r_{l+L} = r_l$ with L from 1 up to 13. The phase diagram resulting from the comparison of the corresponding free energy values and the (assumptive) soliton approximation is given in Fig. 12. The MFA result is exact for the ground state. This is suggested by the coincidence, at $T = 0$, of the minimized MFA free energy with that obtained exactly with the aid of the transfer-matrix method for the corresponding one-dimensional counterpart [17].

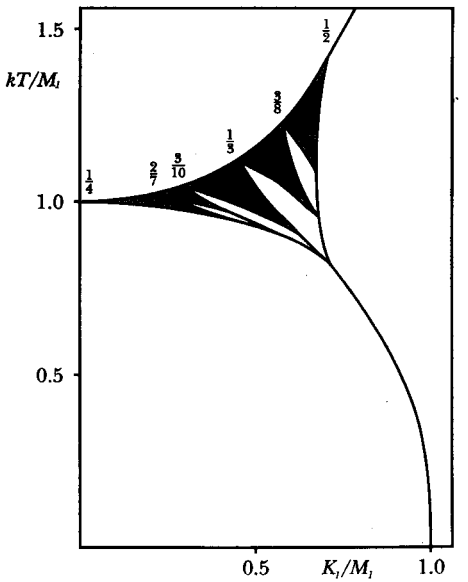

Fig. 12. Phase diagram of the AANNDI model in the MFA, Eq. (25). The modulation vectors of main commensurate phases are given in units of 2π. The shaded area corresponds to longer-period commensurate as well as incommensurate phases. The half-plane $K_1 < 0$ is a mirror image of the half-plane $K_1 > 0$; modulation vectors q should be there replaced by modulation vectors $\frac{1}{2} - q$. After Refs. [3] and [18].

The phase diagram of AANNDI model, Fig. 12, is topologically equivalent to the phase diagram of ANNNI model, Fig. 7. However, physical contents of the free energies (9) and (25) are slightly different. The free energy (9) describes only behaviour of the order parameters n_l; the order parameters m_l are quite independent and can be chosen to behave arbitrarily, *e.g.*, in agreement with experiment. On the contrary, in the free energy (25) the parameters n_l are coupled to the parameters r_l and, through the relations

$$\sigma_i = \omega_i \tau_i, \qquad m_s = \langle \omega_i \tau_i \rangle_{i \in s}, \tag{30}$$

to the parameters m_l. The first of Eqs (30) stems from the first of Eqs (24), regarding the fact that squares of the Ising variables are equal to the unity. Note that from a comparison of relations (24) and (30) it follows that in general $r_l \neq m_l n_l$, unless the approximation (5) is assumed.

For stable solutions of Eqs (26) with $q = 0$ and $q = \frac{1}{2}$ (in units 2π), as well as for the τ-para solution, there is always $r_l = 0$ and $m_l = 0$ [18]. As a consequence, the phase diagram of AANNDI model, Fig. 12, cannot be applied directly for a qualitative explanation of sequences of phase transitions observed in the Classes II, III and V of $A'A''BX_4$ compounds (the phases BF, BA and BC that should correspond to the $q = 0$ or $q = \frac{1}{2}$ phases, and the BP phase that should correspond to the τ-para phase evidently have non-zero σ-orderings). To stabilize non-zero σ-orderings, additional terms

$$J' \sum_{nn'} \sigma_i \sigma_j + L' \sum_{nn'} \sigma_i \tau_i \sigma_j \tau_j \tag{31}$$

can be introduced explicitely into the Hamiltonian (23). The Hamiltonian (23) together with the terms (31) have been analyzed in MFA by the author and Bartkowiak [18] and by Pleimling and Siems [19]. The first term in Equation (31) appeared not nonly to stabilize the σ-orderings but, simultaneously, to expand the region of stability of $q = \frac{1}{4}$ phase in the phase diagram, Fig. 12, at the expense of other modulated phases [18]. Fortunately, the latter effect is compensated by the second term in Eq. (31) [19].

6. Two degrees of freedom per layer

In the previous MFA analysis of the AANNDI model we have assumed either ferro or antiferro orderings of the spins in the hexagonal planes. We reject this assumption now, but to avoid introducing too many variables, we assume a rigidly fixed order of the σ spins of the B type (compare Fig. 6):

$$\sigma_{i\in 1} = -\sigma_{i\in 2} = -\sigma_{i\in 3} = \sigma_{i\in 4} = 1\,. \tag{32}$$

Under such an assumption and on introducing new variables:

$$\begin{aligned} v_l &\equiv -\tfrac{1}{2}(n_{1,l} - n_{2,l}), \qquad w_l \equiv -\tfrac{1}{2}(n_{1,l} + n_{2,l})\,, \\ v_{l+1} &\equiv \tfrac{1}{2}(n_{4,l+1} - n_{3,l+1}), \qquad w_{l+1} \equiv \tfrac{1}{2}(n_{4,l+1} + n_{3,l+1})\,, \end{aligned} \tag{33}$$

the most general MFA free energy for the Hamiltonian (23) extended by the additional terms (31) takes the form

$$\begin{aligned} F^{\mathrm{AANNDI}'}/N &= \sum_l [K_1 v_l v_{l+1} + L_1 w_l w_{l+1} + \tfrac{1}{2} M_1 (v_l w_{l+1} - w_l v_{l+1})] \\ &+ \tfrac{1}{4} kT \textstyle\sum_l [(1 + v_l + w_l)\ln(1 + v_l + w_l) + (1 - v_l + w_l)\ln(1 - v_l + w_l) \\ &+ (1 + v_l - w_l)\ln(1 + v_l - w_l) + (1 - v_l - w_l)\ln(1 - v_l - w_l)]\,, \end{aligned} \tag{34}$$

where N is the number of sites in each hexagonal plane. The parameters K_1, L_1 and M_1 depend in general not only on the parameters K', L' and M', but also on parameters of the remaining interactions as well as on temperature. The fact that neither v_l nor w_l from Eq. (33) vanishes means that we have now two degrees of freedom per each layer of the τ spins.

Taylor expansion of Eq. (34) up to the forth power:

$$F^{\mathrm{AANNDI'}}/N \approx \sum_l [K_1 v_l v_{l+1} + L_1 w_l w_{l+1} + \tfrac{1}{2} M_1 (v_l w_{l+1} - w_l v_{l+1})] + \tfrac{1}{2} kT \sum_l [(v_l^2 + w_l^2) + \tfrac{1}{6}(v_l^4 + w_l^4) + v_l^2 w_l^2] , \tag{35}$$

can be compared with semimicroscopic free energies proposed, on the basis of symmetry analysis, by Chen and Walker [20, 21]:

$$F^{\mathrm{C-W}}/N = \sum_l [\tfrac{1}{2} J v_l v_{l+1} + \tfrac{1}{2} J' w_l w_{l+1} + \tfrac{1}{2}(v_l w_{l+1} - w_l v_{l+1})] + \sum_l [\tfrac{1}{2} a v_l^2 + \tfrac{1}{2} a' w_l^2 + \tfrac{1}{4}(v_l^4 + w_l^4) + \tfrac{1}{2} \gamma v_l^2 w_l^2] , \tag{36}$$

and by Janssen [22, 23]:

$$F^{\mathrm{J}}/N = \sum_l [\tfrac{1}{2} A (x_l^2 + y_l^2) \tfrac{1}{4}(x_l^4 + y_l^4) + B x_l y_l + \tfrac{1}{2} K x_l^2 y_l^2 + C x_l y_{l+1} + D y_l x_{l+1}] . \tag{37}$$

The only difference between Eq. (35) and Eqs (36) and (37) is the number of parameters. Both in Eq. (36) and Eq. (37) there are five parameters whereas in Eq. (35) there are, in fact, only three (one can always renormalize variables, as in Eqs (18)).

The absence of the other two parameters follows from disregarding the coupling of the order parameters v_l and w_l to a possible static distortion of the lattice. The symmetry allowed distortion free energy, including purely elastic quadratic terms, is of the form

$$F^{\mathrm{DIST}}/N = \sum_l (V_2 q_{2,l} v_l + V_3 q_{3,l} w_l + V_4 q_{4,l} v_l w_l) + \sum_l (\tfrac{1}{2} W_2 q_{2,l}^2 + \tfrac{1}{2} W_3 q_{3,l}^2 + \tfrac{1}{2} W_4 q_{4,l}^2) . \tag{38}$$

Normal modes $q_{2,l}$, $q_{3,l}$ and $q_{4,l}$ of lattice distortion are labelled by one-dimensional irreversible representations Γ_2, Γ_3 and Γ_4, respectively, of the

little cogroup C_{2v} for the zone-center wave vector of the layer l [21]. Minimization of the distortion free energy with respect to the distortions $q_{\gamma,l}$:

$$\partial F^{\mathrm{DIST}}/\partial q_{\gamma,l} = 0\,, \tag{39}$$

leads to the relations

$$q_{2,l} = -\frac{V_2}{W_2}v_l, \qquad q_{3,l} = -\frac{V_3}{W_3}w_l, \qquad q_{4,l} = -\frac{V_4}{W_4}v_l w_l\,, \tag{40}$$

which, when put back to Eq. (38), make the terms v_l^2, w_l^2 and $v_l^2 w_l^2$ occur with independent coefficients in the expression for the total free energy $F^{\mathrm{AANNDI'}} + F^{\mathrm{DIST}}$.

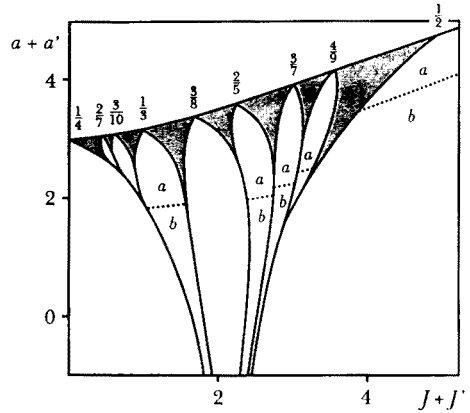

Fig. 13. Phase diagram for the free energy of Chen and Walker, Eq. (36), approximating the AANNDI model free energy in the MFA with two degrees of freedom per layer. It is assumed that $J = J'$, $\gamma = 0$ and $a - a' = 0.8$. The modulation vectors of main commensurate phases are given in units of 2π. The shaded area corresponds to longer-period commensurate as well as incommensurate phases. The half-plane $J + J' < 0$ is a mirror image of the half-plane $J + J' > 0$; the modulation vectors q should be there replaced by $\frac{1}{2} - q$. The dotted lines represent continuous transitions between phases with the same modulation vector distinguished, respectively, by an additional index a or b. The space groups corresponding to particular values of the modulation vector and additional indexes a, b or c (the latter characterizes phases stable in another parameter range) are listed in Table III. Redrawn after Ref. [21].

In Fig. 13 a phase diagram is given, constructed by Chen and Walker [21] after numerical minimization of the free energy (36) for $J = J'$, $\gamma = 0$ and $a - a' = 0.8$. It differs from the phase diagram of the oversimplified version of AANNDI model, Fig. 12, in two respects. First, in the phases with $q = 0$, $q = \frac{1}{2}$ (in units 2π) and in the para phase we have now,

by assumption (Eq. (32)), a non-vanishing σ-order. And secondly, there are additional continuous phase transitions within phases with the same modulation vector q, represented in Fig. 13 by dotted lines. In order to distinguish different phases with the same modulation vector q, additional labels a, b and c are introduced (in the original paper by Chen and Walker [21] they are denoted as I, II and III, respectively). Table III gives the space groups corresponding to particular commensurate values of the modulation vector and particular additional labels.

TABLE III

Space groups of commensurate phases described by the free energy (36) (after Ref. [21])

Modulation vector/2π	(Additional label) and space group
$q = (2s+1)/2(2t+1)$	(a) $P112_1/n$, (b) $P2_12_12_1$, (c) $P112_1$
$q = s/(2t+1)$	(a) $Pc2_1n$, (b) $P2_1/c11$, (c) $Pc11$
$q = (2s+1)/4t$	(a) $P12_1/c1$, (b) $P2_1cn$

Note: s and t are arbitrary integers

The free energy (36) not only describes the same observed sequences of changes of the modulation vector with temperature as the ANNNI model does, Figure 8, but also determines the space groups of the corresponding phases. Moreover, it can explain transitions between different phases of the same modulation vectors, marked in Figures 3 and 4 with an asterisk. The low-temperature transition to the ferri ordered $P\bar{1}$ ($Z = 4$) phase observed in caesium compounds, Fig. 5, also has such a character. All observed transitions of that type are listed in Table IV.

TABLE IV

Experimentally observed transitions between phases with the same vector of modulation along the hexagonal c-axis.

q_{red}/c^*	$q_{ext}/2c^*$	Z	Transition	Compounds
1/3	1/3	12	$P2_1cn \rightarrow P1c1$	Rb_2ZnBr_4
1/4	3/8	16	$P2_1n \rightarrow Pc11$	$(NH_4)_2ZnCl_4$
1/3	1/6	12	$P112_1/n \cdots P2_12_12_1$	T_2ZnCl_4, T_2CoCl_4
0	1/2	4	$P112_1/n \rightarrow P\bar{1}$	Cs_2HgBr_4, Cs_2CdBr_4, Cs_2CdI_4

Note: for relation between the reduced and the extended zone modulation vectors, q_{red} and q_{ext}, respectively, see Fig. 8 caption.

We conclude this section with a statement that both the ANNNI model, Eq. (8), and the AANNDI model, Eq. (23) and (31), can describe all the observed phase transitions in $A'A''BX_4$ compounds involving longer-period or incommensurate modulations of structure along the hexagonal c-axis. However, in order for the description be adequate, one has to assume that interactions not explicitely considered in the models allow ferri-type orderings in hexagonal planes. This means that in the corresponding MFA free energies two degrees of freedom per layer for the order parameter must be taken into account. Chen and Walker [21] performed an analysis of the free energy corresponding, under these additional assumptions, to the AANNDI model. The same can be done for the ANNNI model. Both models describe to some degree the actual situation in $A'A''BX_4$ compounds, though the AANNDI model seems to be more close to reality, as interactions between nearest neighbours are usually much stronger than those between next-nearest ones. Anyway, a general theory offers such a large number of parameters than any attempt at its quantitative adjustment to the experimental data is, at present, ambiguous, and so without any methodological significance.

7. Longer-period modulations in the hexagonal plane

Apart from many cases of long-period modulations of the structure along the hexagonal axis, a group (though less numerous) of longer-period modulations in the hexagonal plane were also observed in $A'A''BX_4$ compounds (Classes I, II, IV and VI, and $LiNH_4SO_4$ in Class V, Figs 3 to 5). The simplest example of such modulations are ferri and partially disordered antiferro structures corresponding to triple-q and double-q modulations of the order parameter in the hexagonal plane with the modulation vector value $|q| = \pi$ (Fig. 14; the antiferro ordering in the hexagonal plane considered in Section 3 correspons to a single-q modulaton).

One obvious mechanism of longer-period modulations in the hexagonal plane is a competition between the nearest- and the next-nearest-neighbour interactions between spins in these planes (note that the nnn pairs in the hexagonal planes are the fourth-neighbour pairs from the point of view of the whole hcp structure, see Fig. 6). Restricting our considerations to the single σ Ising subsystem and denoting by J_1 and J_2 the parameters of the nn and the nnn interactions, respectively, in the triangular lattice of sites in each hexagonal plane ($J_1 \equiv J$), we consider the Hamiltonian:

$$\mathcal{H}^{\mathrm{PNNNI}} = J_1 \sum_{\mathbf{nn}} \sigma_i \sigma_j + J_2 \sum_{\mathbf{nnn}} \sigma_i \sigma_j - H \sum_i \sigma_i \,. \tag{41}$$

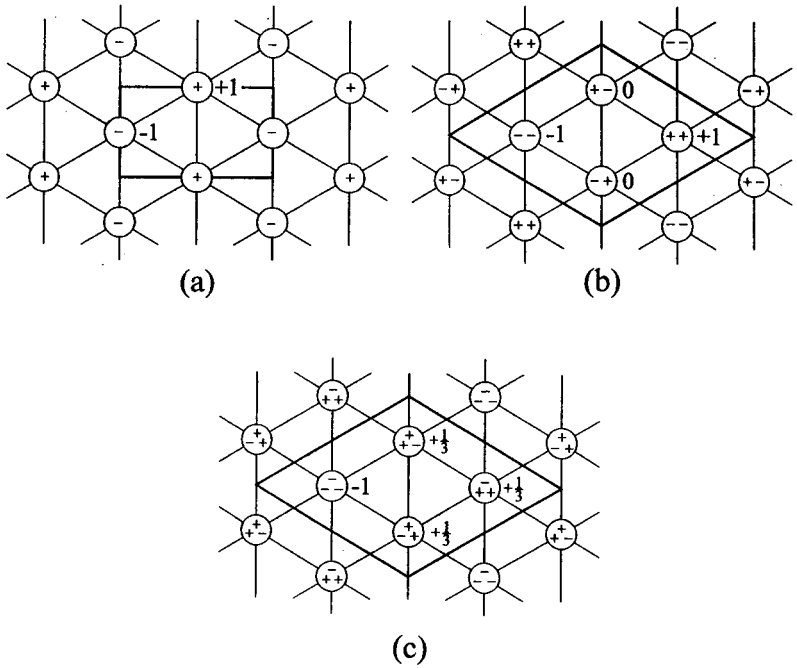

Fig. 14. Single-q, double-q and triple-q modulations of the order parameter on the triangular lattice with $|q| = \pi$. Resultant orderings are antiferro, partially disordered antiferro, and ferri ones, respectively. The corresponding elementary cells are marked with bold lines.

In analogy to the ANNNI model, Eq. (8), we refer to Eq. (41) as the PNNNI (planar next-nearest-neighbour Ising) model, though this terminology is not commonly used. Nontrivial effects in the PNNNI model can be due to the external field H term. No additional interactions outside the plane are necessary.

Thermodynamics of the PNNNI model on the triangular lattice was studied by a number of authors, among which we mention Kaburagi and Kanamori [24], Nakanishi and Shiba [25, 26], Saito, Furata and Hojou [27], and Matsubara and Inawashiro [28]. All the orderings stable at $T = 0$ are shown in Fig. 15, and in Fig. 16 the groud-state MFA phase diagram for the Hamiltonian (41), found by Kaburagi and Kanamori [24], is given. The partially disordered antiferro structures, denoted as PD1, PD2 and PD3, are stable only marginally. However, for finite temperatures the region of stability of these phases expands [26–28].

Table V presents five experimentally observed cases of longer period modulations in the hexagonal plane. Four cases of commensurate modula-

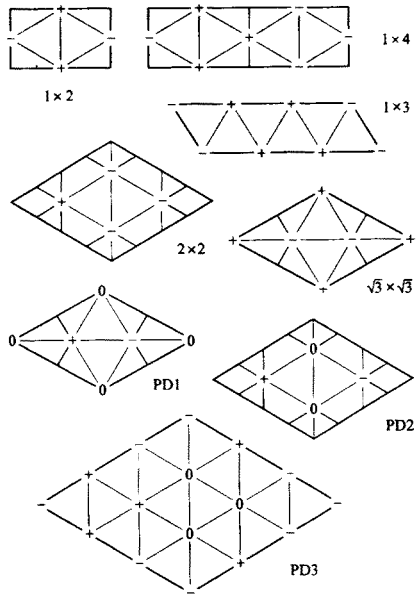

Fig. 15. Possible ground-state orderings for the PNNNI model, Eq. (41), on the triangular lattice. Boundaries of elementary cells are marked with bold lines; thin lines join the neighbouring spins. Three types of partially disordered antiferro structures are also shown.

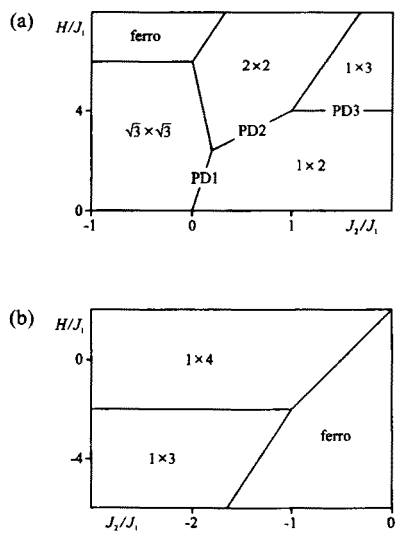

Fig. 16. Ground-state MFA phase diagram of the PNNNI model, Eq. (41), on the triangular lattice for positive (a) and negative (b) nn interaction parameter J_1. All transitions are discontinuous. Notation of phases is explained in Figure 15. After Ref. [24], modified. The partially disordered antiferro phases PD1 [28], PD2 [27] and PD3 [26] are stable along the border of fully ordered antiferro 1×2 phase.

tions, when restricted to a single layer and a single kind of spins, can be interpreted in terms of three types of orderings provided by the PNNNI model. These are the PD2, the 2×2 and the 1×4 orderings. In all three cases the elementary cell contains four sites per layer. Note that the PD2 and the 2×2 orderings are stable only in non-zero external fields.

TABLE V

Experimentally observed crystallographic phases with longer period modulation in the hexagonal plane.

Phase	Modulation vector	Compounds
incommens.	q along b^*	K_2MoO_4, K_2WO_4, Rb_2WO_4
$C1c1$ ($Z = 24$)	$q = (a^* + b^*)/2$	Rb_2BCl_4 and K_2BCl_4, B = Zn, Co
$Pbc2_1$ ($Z = 8$)	$q = b^*/2$	Class IV
$C1c1$ ($Z = 16$)	$q = (a^* + b^*)/2$	$LiNH_4SO_4$
?	$q = (a^* + b^*)/2$?	Class VI

The $C1c1$ phases with the modulation vector $q = (a^* + b^*)/2$, observed in $LiNH_4SO_4$ and the Class II compounds, can be considered as the PD2 phase of the PNNNI model, assuming that the spins σ in Eq. (41) are replaced by the spins $\omega \equiv \sigma\tau$. An effective external field can be considered as originating from $\sigma_i\sigma_j \equiv \omega_i\tau_i\omega_j\tau_j$ or $\tau_i\tau_j \equiv \omega_i\sigma_i\omega_j\sigma_j$ interactions.

The high-temperature intermediate phase observed in the Class VI compounds ($LiKSO_4$ and $LiRbCrO_4$, Fig. 5), also probably with the modulation vector $q = (a^* + b^*)/2$, was interpreted either as the 2×2 phase of the PNNNI model with a triple-q modulation, or the phase PD2 with a double-q modulation, but the correct interpretation seems to be the latter one [29]. In this case the spins of the PNNNI model coincide with our σ spins; an effective external field can origin from $\sigma_i\tau_i\sigma_j\tau_j$ interactions.

The $Pbc2_1$ ($Z = 8$) phase with the modulation vector $q = b^*/2$ observed in the Class IV compounds can be considered as the 1×4 phase of the PNNNI model assuming that the spins σ_i are replaced by the spins $\omega_i \equiv \sigma_i\tau_i$. Here no effective external field is necessary.

Incommensurate structural modulations in the hexagonal plane were observed in K_2MoO_4 and tungstates, Class I of compounds, and in K_2ZnCl_4 (Fig. 3). The PNNNI model provides such incommensurate modulations for finite temperatures [26].

An alternative model to the PNNNI one is the PANNDI (planar antisymmetrical nearest-neighbour Ising) model [5, 18] with the Hamiltonian in

the simplest version consisting of the two terms:

$$\mathcal{H}^{\mathrm{PANNDI}} = J \sum_{\mathrm{nn}} \sigma_i \sigma_j + \tfrac{1}{2} M \sum_{\mathrm{nn}} \sigma_i \sigma_j (\tau_i - \tau_j) . \tag{42}$$

This seems to give a more realistic mechanism of longer period modulations in the plane than that offerred by the PNNNI model as the nn interactions are certainly stronger than the nnn ones. Unfortunately, no detailed analysis of the PANNDI model has been performed yet. As for long-period modulations along the hexagonal axis, also for long-period modulations in the hexagonal plane we refrain from any attempt at quantitative adjustment of models to the experimental data. Both the PNNNI and the PANNDI models are, however, worth studying from the theoretical point of view.

8. Summary

A simple statistical model being a subject of this review explains practically all structural phase transitions observed in a large group of crystalline compounds of a general chemical formula $A'A''BX_4$. Phase transitions in these compounds result from various orientational orderings of BX_4 groups. There are four discrete orientational states of each BX_4 tetrahedron in the cationic environment. The model labels them with the help of two Ising variables: $\sigma = \pm 1$ (positions of the tetrahedron with one of the apices up or down the distinguished hexagonal axis) and $\tau = \pm 1$ (turns of the tetrahedron to the right or left about this axis). Experimental structural data for $A'A''BX_4$ compounds are reviewed in Figs 3 to 5. Interpretation of these data in terms of the presented model is given in Tables I to V and in Fig. 8.

Symmetrical nearest-neighbour interactions between spins on the prototype hcp structure can stabilize 25 various, at most four-sublattice, orderings. Eight of them were found in $A'A''BX_4$ compounds (Table I).

Longer-period or incommensurate structural modulations along the hexagonal c-axis result from the next-nearest-neighbour τ-τ interactions or, competitively, antisymmetrical nearest-neighbour $\tau\sigma$-τ interactions. The phase diagrams of the corresponding ANNNI (axial next-nearest-neighbour Ising) and AANNDI (axial antisymmetrical nearest-neighbour double Ising) models are given in Figs 7 and 12, respectively. In Fig. 8 a quantitative fitting of most sequences of transitions is shown on the example of ANNNI model. Stabilization or destabilization of the phase with $q = \frac{2}{5} c^*$ observed in several compounds are probably due to an effective field originating from the symmetrical σ-τ coupling. An alternative explanation is offered by the model with further distance interactions or two derivatives of the ANNNI model: the DIFFOUR (discrete frustrated φ^4) model, Fig. 9, and the ELRII (effective long-range interaction Ising) model, Fig. 10.

To determine the space groups of the modulated phases, two degrees of freedom per each plane of spins have to be assumed in all models. Analysis of a derivative of the AANNDI model under such an assumption (Fig. 13 and Table III) enabled one to explain also transitions between phases with the same modulation vector (Table IV).

Longer-period modulations of the structure in the hexagonal plane can be explained as resulting from the next-nearest-neighbour σ-σ interactions in the hexagonal planes being, from the point of view of the whole hcp lattice, only the fourth-neighbourhood interactions. The corresponding PNNNI (planar next-nearest-neighbour Ising) model describes two main kinds of the observed commensurate modulations identified as a double-q modulation with $|q| = \pi$ and a single-q modulation with $|q| = \pi/2$ (Table V and Figs 14 to 16). Preasumably a mechanism of longer-period modulations in plane more realistic than that offerred by the PNNNI model can give the PANNDI (planar antisymmetric nearest-neighbour double Ising) model, but no detailed analysis of it has been performed yet.

My thanks for discussions and cooperation go to Mirosław Bartkowiak, Robert Farhi, Michael Glaser, Mohamed Halawa, Teodor Krajewski, Philippe Moch, Michel Pleimling, Marguerite Quilichini and Rolf Siems. The study has been supported in part by the Alexander von Humboldt Foundation and the Polish State Commitee for Scientific Research (Project 2 0062 91 01).

REFERENCES

[1] H.Z. Cummins, *Phys. Repts.* **185**, 211 (1990).
[2] P.E. Tomaszewski, *Phase Transitions* **38**, 127 (1992).
[3] M. Kurzyński, *Phase Transitions* **52**, 1 (1994).
[4] M. Kurzyński, M. Halawa, *Phys. Rev.* **B34**, 4846 (1986).
[5] M. Kurzyński, *Ferroelectrics* **78**, 121 (1988).
[6] Y. Yamada, N. Hamaya, *J. Phys. Soc. Japan* **52**, 3466 (1983).
[7] P. Bak, *Rep. Prog. Phys.* **45**, 587 (1982).
[8] W. Selke, *Phys. Repts.* **170**, 213 (1988).
[9] S. Aubry, in *Solitons and Condensed Matter Physics*, eds. A. R. Bishop and T. Schneider, p. 264., Springer, Berlin 1978.
[10] T. Janssen, J. A. Tijon, *Phys. Rev.* **B25**, 3767 (1982).
[11] T. Janssen, A. Janner, *Adv. Phys.* **5**, 519 (1987).
[12] T. Janssen, *Ferroelectrics* **66**, 203 (1986).
[13] J. Villain, M.B. Gordon, *J. Phys. C* **13**, 3117 (1980).
[14] F. Axel, S. Aubry, *J. Phys. C* **14**, 5433 (1981).
[15] H. Mashiyama, *J. Phys. C* **16**, 187 (1983).

[16] K. Kawamura, A. Kuramashi, H. Nakamura, H. Kasano, H. Mashiyama, S. Nakanishi, H. Itoh, *Ferroelectrics* **105**, 279 (1990).
[17] M. Kurzyński, M. Ossowski, M. Bartkowiak, *Ferroelectrics* **105**, 107 (1990).
[18] M. Kurzyński, M. Bartkowiak, *J. Phys.: Condens. Matter* **4**, 2609 (1992).
[19] M. Pleimling, R. Siems, *Ferroelectrics* **151**, 69 (1994).
[20] Z.Y. Chen, M.B. Walker, *Phys. Rev. Lett.* **65**, 1223 (1990).
[21] Z.Y. Chen, M.B. Walker, *Phys. Rev.* **B43**, 5634 (1991).
[22] T. Janssen, *Ferroelectrics* **124**, 41 (1991).
[23] T. Janssen, *Z. Phys.* **B86**, 277 (1992).
[24] M. Kaburaki, J. Kanamori, *J. Phys. Soc. Japan* **40**, 291 (1976).
[25] K. Nakanishi, H. Shiba, *J. Phys. Soc. Japan* **51**, 2089 (1982).
[26] K. Nakanishi, *J. Phys. Soc. Japan* **52**, 2449 (1983).
[27] Y. Saito, K. Furuta, M. Hojou, *J. Phys. Soc. Japan* **56**, 178 (1987).
[28] F. Matsubara, S. Inawashiro, *J. Phys. Soc. Japan* **56**, 2666 (1987).
[29] M.A. Pimenta, P. Echegut, Y. Luspin, G. Hauret, F. Gervais, *Phys. Rev.* **B39**, 3361 (1989).